A Singular Molecule-to-Molecule Transformation on Video: The Bottom-Up Synthesis of Fullerene C-60 from Truxene Derivative C60H30

ACSNANO

www.acsnano.org

ARTICLE

A Singular Molecule-to-Molecule Transformation on Video: The Bottom-Up Synthesis of Fullerene C_{60} from Truxene Derivative $C_{60}H_{30}$

Dominik Lungerich,* Helen Hoelzel, Koji Harano, Norbert Jux, Konstantin Yu. Amsharov, and Eiichi Nakamura*

Cite This: *ACS Nano* 2021, 15, 12804–12814

Read Online

ACCESS | Metrics & More | Article Recommendations | Supporting Information

ABSTRACT: **Singular reaction events of small molecules and their dynamics remain a hardly understood territory in chemical sciences since spectroscopy relies on ensemble-averaged data, and microscopic scanning probe techniques show snapshots of frozen scenes. Herein, we report on continuous high-resolution transmission electron microscopic video imaging of the electron-beam-induced bottom-up synthesis of fullerene C_{60} through cyclodehydrogenation of tailor-made truxene derivative 1 ($C_{60}H_{30}$), which was deposited on graphene as substrate. During the reaction, $C_{60}H_{30}$ transformed in a multistep process to fullerene C_{60}. Hereby, the precursor, metastable intermediates, and the product were identified by correlations with electron dose-corrected molecular simulations and single-molecule statistical analysis, which were substantiated with extensive density functional theory calculations. Our observations revealed that the initial cyclodehydrogenation pathway leads to thermodynamically favored intermediates through seemingly classical organic reaction mechanisms. However, dynamic interactions of the intermediates with the substrate render graphene as a non-innocent participant in the dehydrogenation process, which leads to a deviation from the classical reaction pathway. Our precise visual comprehension of the dynamic transformation implies that the outcome of electron-beam-initiated reactions can be controlled with careful molecular precursor design, which is important for the development and design of materials by electron beam lithography.**

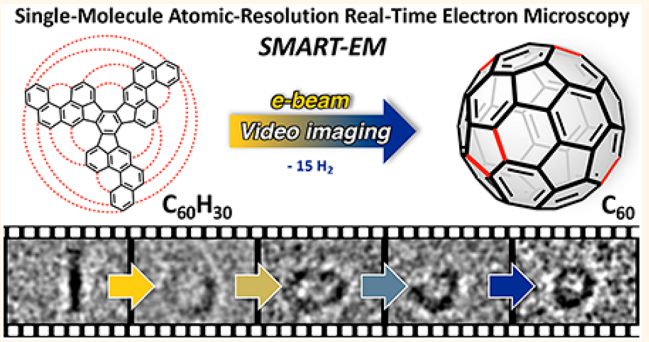

KEYWORDS: *cyclodehydrogenation, polycyclic aromatic hydrocarbon, fullerene, single-molecule dynamics, DFT-modeling, transmission electron microscopy*

With its discovery in 1985,[1] C_{60} fullerene emerged as one of the most iconic organic molecules, which, since then, appealed as a vastly explored moiety in various energy,[2] nanomaterials,[3] and biomedical applications[4] and, last but not least, as a fascinating total synthesis target for the organic chemist.[5] In this respect, groundbreaking results, which launched the successful preparative synthesis of Buckminsterfullerene,[6] were produced by Scott, Drewello, and co-workers in 2001. By laser ablation of preprogrammed polycyclic aromatic hydrocarbon (PAH) **1** ($C_{60}H_{30}$), they achieved the directed synthesis of fullerene C_{60} *via* consecutive cyclodehydrogenation in the mass spectrometer.[7] These insights, obtained from gas-phase experiments, initiated the successful bottom-up synthesis of C_{60} on the preparative scale.[6]

Afterward, with the advancement of scanning probe microscopy techniques, the process of addressing chemical reactions reached quickly molecular level resolution, as demonstrated in 2008 by Otero, Biddau, and co-workers. They transformed, on an active Pt(111) surface, **1** to C_{60}[8] and visualized subsequently the outcome by scanning tunneling microscopy. Certainly, the direct microscopic visualization of molecules

Received: March 15, 2021
Accepted: May 18, 2021
Published: May 21, 2021

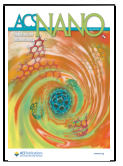

https://doi.org/10.1021/acsnano.1c02222
ACS Nano 2021, 15, 12804–12814

pleases not only the human eye but also confirms unambiguously the results with atomic precision.[9] More importantly, the microscopic elucidation of this chemical transformation avalanched the success of surface-mediated syntheses of molecules and materials, which are nowadays controlled with outstanding precision.[10−12]

However, information on the continuous dynamics of these processes from scanning-probe techniques can be extracted only to a limited extent. Hereby, substantial progress in the field of transmission electron microscopy (TEM) was made within the past decade. In the literature often described as single-molecule atomic-resolution real-time electron microscopy ("SMART-EM") or "chemTEM",[13,14] the direct imaging technique revealed to be especially powerful in the initiation and capture of nonrepetitive events.[15,16] For example, the formation of buckyballs from bilayered graphene, which reflects the top-down fullerene formation during the arc-discharge synthesis, was demonstrated in 2010 by Chuvilin *et al.*[17] Further recent highlights comprise the bimolecular reaction of fullerenes,[18,19] the reactivity of endohedral fullerenes and their entrapped molecules,[20] the transformations of polycyclic aromatic hydrocarbons to oligomers,[21−23] the analysis of reactive metal clusters,[24−26] the bonding character of dimeric metal atoms,[27] and even the emerging nucleation of a NaCl nanocrystal.[28] Yet, a discrete multistep synthesis (molecule-to-molecule transformation), which leads to the predicted product and does not terminate in the formation of polymers, was never captured.[21]

Herein, we report on the video imaging by transmission electron microscopy of the bottom-up transformation of truxene derivative **1** to C_{60} fullerene, which encompasses a total of 15 cyclodehydrogenation steps (Figure 1). Continuous

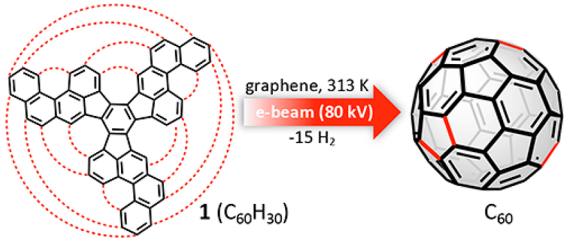

Figure 1. SMART-EM video-imaging of the electron-beam-induced cyclodehydrogenation of preprogrammed precursor 1 to C_{60}.

video imaging allows for the structural analysis and monitoring of formed intermediates in real-time. Unlike in the case of frequently studied fullerenes[16,18−20,29−34] or PAHs[21−23,35−37] entrapped in carbon nanotubes, our molecule is found as an isolated entity on a graphene monolayer. This circumstance prevents the oligomerization process with other fullerenes or molecules and allows us to focus solely on the intramolecular processes in granular detail. Through the identification of discrete molecular structures, we aim to understand, whether electron-beam-induced events can be designed, and to what extent they can be predicted from an organic chemist's point of view. Understanding these processes not only is of high value to the comprehension of fundamental chemistry but also is directly related to technological applications, utilizing electron beam lithography for the construction of nanoarchitectures.[38]

RESULTS AND DISCUSSION

TEM Analysis. We aimed for C_{60}, as fullerenes represent well-explored candidates in electron microscopy studies, and the size and shape can be easily identified.[17−19,39] For our purpose, we synthesized compound **1** (Figure S1), which can be considered as a benchmark molecule for the C_{60} formation.[6,7,40,41] We drop-casted a 10^{-5} M solution of **1** in toluene, on a dry-cleaned graphene-coated gold grid (Figure S2),[42] the excess solution was removed, and the grid was dried in high vacuum (10^{-5} Pa), before introducing it into the TEM chamber. Traces of remaining volatiles were removed in the TEM by heating the grid to 473 K for 1 h, before exposure to electron irradiation. SMART-EM observations were carried out with an aberration-corrected TEM (JEM-ARM200F) at 313 ± 5 K at magnifications of 1000k. The acceleration voltage was set to 80 kV, and the camera frame rate was kept at 2 fps.

After scanning the graphene surface for viable candidates, we discovered an isolated, single molecule of **1**, as depicted in Figure 2 and Supporting Information Video S1, suitable for detailed investigation. It was found to be covalently bound to the graphene monolayer (GML), which prevents fast translations on the surface as well as the desorption of the molecule. At the same time, the remote attachment of **1** on the monolayer prevents disturbing interactions or side reactions with other forms of hydrocarbons that are found to be adsorbed on the surface. From the alignment of the graphene lattice and the angle of the molecular direction (Figure 2a and Figure S3), we can limit the binding to the armchair direction of the graphene lattice as depicted in Figure 2b.[43] The observed rodlike structure in Figure 2c, which persists for over 44 s, measures on average 1.18 nm (±0.05), as determined from single-molecule statistics between 0.5 and 44 s (compare Figures S4−S7). The corresponding electron dose-corrected EM image simulations of respective models, depicted in Figure 2 d−g, suggest from size, shape, and contrast that the molecule is bound *via* cycloaddition at the 3,4-position as depicted in Figure 2d. This finding is also supported by density functional theory (DFT) calculations, which favor the 3,4 over the 2,3-position (Table S2). However, the exact binding motif of the cycloaddition reaction to the graphene surface ([2+2] or [4+2]) cannot be differentiated, as both models fit well within the obtained standard deviation (σ = 0.05 nm) and intrinsic pixel resolution (0.0211 nm). Our findings are consistent with reports by Chamberlain *et al.*, who showed that perchlorinated coronene reacts in a Diels−Alder reaction with the GML in the TEM.[21] Nonetheless, the same binding motifs at the 2,3-position, as shown in Figure 2e, can be excluded with high certainty. Also, the [2+3] cycloaddition (Figure 2f) at the zigzag periphery (4,5-position) and the covalent attachment through a C−C single bond at the 3-position (Figure 2g) do not match the observed TEM images in size and shape and can be therefore excluded.[43,44] Details are shown in Figure S8.

With the identified nature of chemisorbed precursor **1** at the 3,4-position ($C_{60}H_{28}$), the first severe molecular transformation takes place between t = 45.0−49.0 s. As shown in the image series in Figure 3a, a dynamic structural deformation to a seemingly spherical structure is observed. The intermediate measures 0.82 nm (±0.03) in diameter and, thus, is too large to be C_{60}, yet. In Figure 3b and Figure S9, this spherical intermediate shows a good correlation with a surface-bound bowl-shaped model of the constitution $C_{60}H_{14}$, which amounts to six newly formed C−C bonds and two new bonds

https://doi.org/10.1021/acsnano.1c02222
ACS Nano 2021, 15, 12804−12814

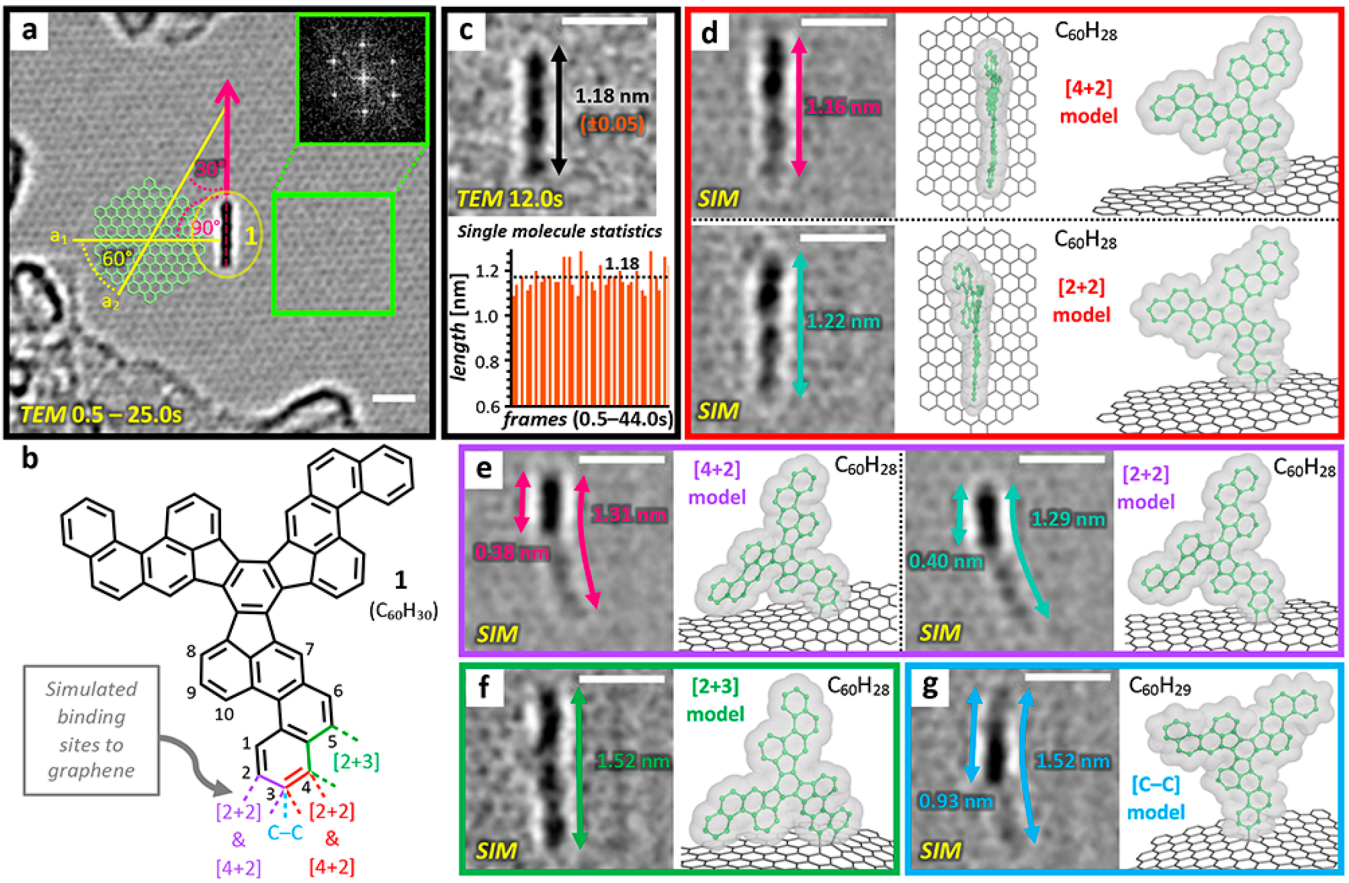

Figure 2. SMART-EM exploration of precursor 1 bound to the graphene monolayer. All TEM images and simulations are consistently band-pass and Gauss blur filtered throughout the text: scale bar (white) 1 nm; EM simulations are electron dose corrected (3.0×10^5 e^- nm^{-2} s^{-1}); chemical models are represented as Z^2-adjusted models,[15] with a transparent CPK surface throughout the text. (a) Overview of the first 25 s of scene and binding angle on GML; 50 frames stack (25 s exposure time). Inset shows FFT diffraction pattern obtained from monolayer area highlighted in light green. (b) Structure of 1; colored bonds represent the binding sites in the respective simulations in (d–g). (c) 1 bound to graphene at t = 12.0 s, and statistical analysis of molecular length. (d) Best-fitting EM simulation of 1 ($C_{60}H_{28}$) bound to graphene *via* [4+2] (top) or [2+2] (bottom) cycloaddition at the 3,4-position. (e) EM simulation of [4+2] (left) or [2+2] (right) cycloaddition model at the 2,3-position. (f) EM simulation of [2+3] model at the 4,5-position. (g) EM simulation of 1 ($C_{60}H_{29}$) bound *via* C–C single bond at the 3-position.

to the GML. The identified intermediate agrees with the thermochemical analysis of the gas-phase calculated $C_{60}H_{18}$ intermediate (*vide infra*). The intermediate lasts for about 3 s before it starts to migrate over the graphene surface (Figure 3c and Figure S10). Determined from center-of-mass analysis, the migration distance is around 0.3 nm and reflects the dynamic and reversible C–C binding behavior of the molecule to the surface. This short-lived intermediate undergoes further morphological changes to an oval-shaped intermediate as shown in Figure 3d (Figures S11–S13). With its dimensions of 0.92 × 0.63 nm, this intermediate is best described by a model, resembling a partially dehydrogenated hemifullerene with the constitution $C_{60}H_5$. Dehydrogenated terminal carbon atoms of organic materials have been described in TEM studies before.[45,46] While H atoms do not contribute significantly to the contrast of molecules in TEM, their presence greatly contributes to the overall shape and dimensions of the molecule (*vide infra* and compare Figure S14). After a period of 9 s, the structure appears to open up again to a half-circle structure, as shown in Figure 3e (Figure S15). Simulations of a hemifullerene intermediate ($C_{60}H_3$) suggest that the molecule underwent an on-surface rearrangement. From here on, this heavily dehydrogenated reactive intermediate undergoes rapid shape-shifting motions. In Figure 3f, the structure undergoes a reversible linearization from a rod- to bent-shaped structure, before it quickly cyclizes to a "D"-shaped structure in Figure 3g. Finally, the intermediate coalesces to a stable spherical structure that remains stable for >25 s until the end of the video (Figure 3h and Figures S16–S19). With its contrast, shape, and size (outer diameter: 0.63 ± 0.04 nm), this structure resembles C_{60} fullerene and agrees with a C_{60} model bound *via* [4+2] cycloaddition at the reactive [6,6] double bond to the GML (compare alternatives in Figures S20–22).[47] In analogy to the active metal surface-assisted reactions of C_{60},[8] the fullerene is covalently bound to the graphene layer, which explains its limited mobility during the observation. Detachment from the graphene surface is not observed for the period of 138 s of the video, after which up to 8.5×10^7 e^- nm^{-2} were emitted. Another already formed C_{60} molecule was recorded for 100 s (end of the recording) without any sign of decomposition (compare Video S2).

Computational Analysis. To shed light on the electron-beam-induced formal 15-fold oxidative cyclodehydrogenation reaction of tailor-made **1** to C_{60}, we carried out a thermochemical analysis on the M06-2X-def2-TZVP level of density functional theory (DFT). In particular, we were

https://doi.org/10.1021/acsnano.1c02222
ACS Nano 2021, 15, 12804–12814

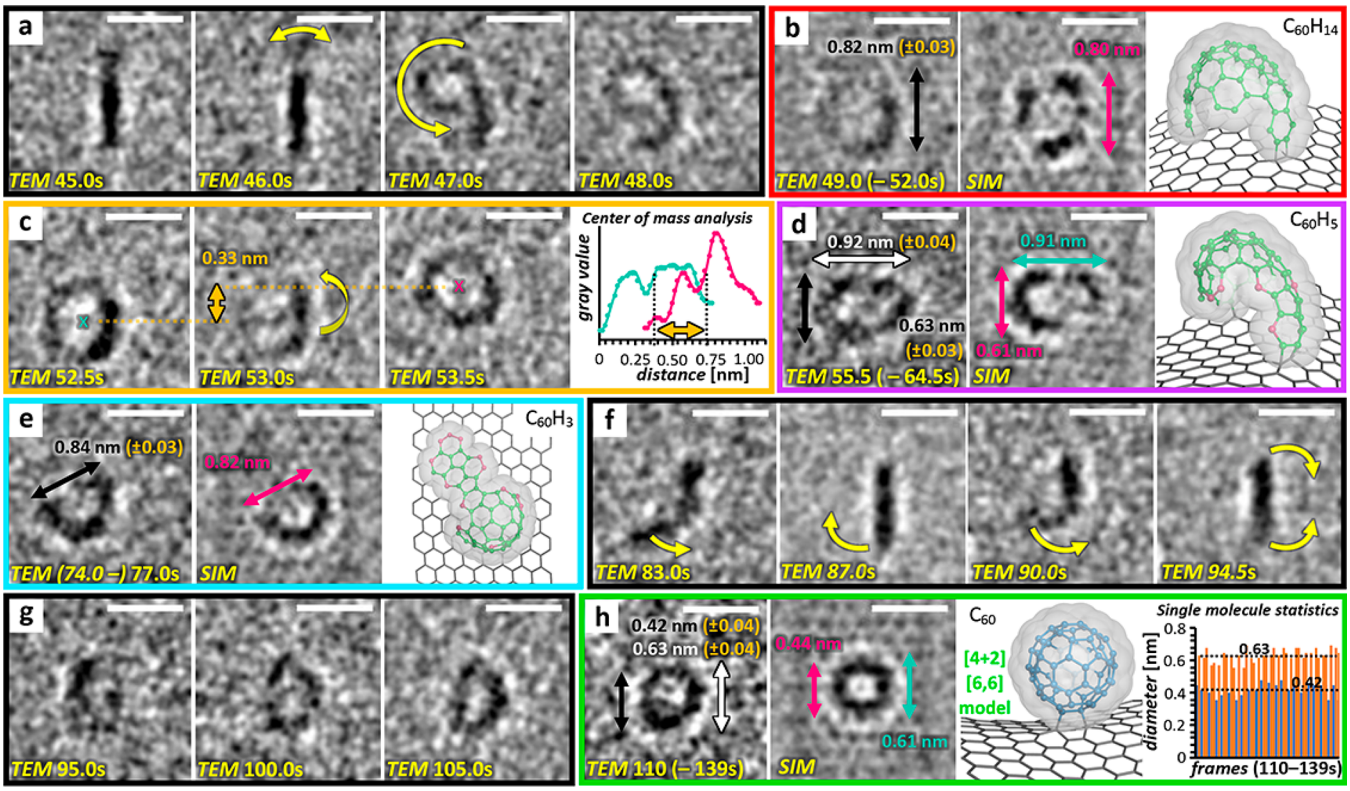

Figure 3. SMART-EM exploration of molecule-to-molecule transformation of 1 to C_{60} on graphene. Yellow arrows indicate direction of motion. (a) First severe structural deformation. (b) Spherical intermediate; simulation suggests a hemifullerene model ($C_{60}H_{14}$), with hydrogenated secondary C atoms. (c) On-surface translation of spherical intermediate determined from center of mass shift. (d) Oval-shaped intermediate; simulation suggests a hemifullerene model ($C_{60}H_5$). Atoms in red indicate dehydrogenated secondary C atoms. (e) Half-circle-shaped intermediate; simulation suggests an on-surface rearranged hemifullerene model ($C_{60}H_3$). (f) Repetitive, and vivid stretching and bending of reactive intermediate. (g) Transformation to a "D"-shaped intermediate. (h) Final formation of a spherical structure; simulation suggests a C_{60} model chemisorbed *via* [4+2] cycloaddition to the GML.

interested in the formation of the spherically shaped intermediate (compare Figure 3b), which was simulated to be a hemifullerene with four C−C bonds to graphene and a constitution of $C_{60}H_{14}$. The subsequent 6-fold cyclodehydrogenation of **1** to $C_{60}H_{18}$ can proceed through 48 intermediates, of which 13 belong to the $C_{60}H_{18}$ constitution. However, one of the energetically favored pathways, depicted in Figure 4a, leads to isomer $\mathbf{C_{60}H_{18}(h)}$, which is found to be the parent isomer of the best-fitting simulated structure as depicted in Figure 4b. This finding suggests that, up to that intermediate, the chemical transformation is thermodynamically and kinetically controlled (*vide infra*). While transformations to other isomers can require up to 2.5 eV, the energetically preferred pathway requires typically below 1.8 eV per step. The complete thermochemical summary is shown in Figure 4c, which reveals an average energy of 1.4 eV per reaction step and a total energy consumption of 20.5 eV for the complete synthesis of C_{60} from **1**. The full thermochemical analysis of **1** to C_{60} as well as all considered isomers are found in the Supporting Information in Tables S7−S9.

Even though the reaction pathway to intermediate $\mathbf{C_{60}H_{18}(h)}$ appears to be coherent with the thermochemical data, the reaction mechanism can follow different pathways to yield the same product. The currently most widely accepted mechanism for e-beam-induced reactions in single-molecule studies is the so-called knock-on energy transfer mechanism, where the electrostatic interaction of the beam electron with the nucleus of the atom leads to a kinetic energy transfer *via* elastic scattering, as depicted in Figure 5a. The absorbed energy leads subsequently to respective bond vibrations and, in the case of exceeding the bond threshold energy E_d, to a homolytic bond cleavage. Hereby, the transferred energy E_T is dependent on the intrinsic kinetic energy of the electron E_0, the mass of the atom A, and the elastic scattering angle θ, as expressed in eq 1 in Figure 5a. At this point, it should be mentioned that , unlike in the depiction in Figure 5a, the vast majority of electrons is scattered at an angle below 5°, as indicated in Figure 5b by the differential elastic-scattering cross-section for hydrogen at 80 keV kinetic energy. Recently, Biskupek *et al.* demonstrated that the absorbed energy E_T of an atom 1 can be further passed to a second atom 2 to give E'_T, which follows the relationship expressed in eq 2 in Figure 5a.[20] The relationship between the e-beam energy uptake of carbon and hydrogen atoms and the transfer to a second atom as a function of acceleration voltage is shown in Figure 5b. Hereby, it becomes evident that, at the utilized acceleration voltage of 80 kV, a homolytic C−H bond cleavage ($E_d \approx 7.6$ eV, compare Table S4) can occur only upon direct electron−hydrogen atom interaction, whereas secondary energy transfer processes from carbon to hydrogen atoms reach only a value of $E'_{max} \approx 4.5$ eV, which leads to mere vibrational excitation. The heterolytic bond cleavage into ion pairs is in the herein discussed case energetically unfavored (compare Table S6).

With the given set of possible transferable energies, several reaction mechanisms can be envisioned. For that purpose, we calculated the knock-on induced bond dissociation energies,

https://doi.org/10.1021/acsnano.1c02222
ACS Nano 2021, 15, 12804−12814

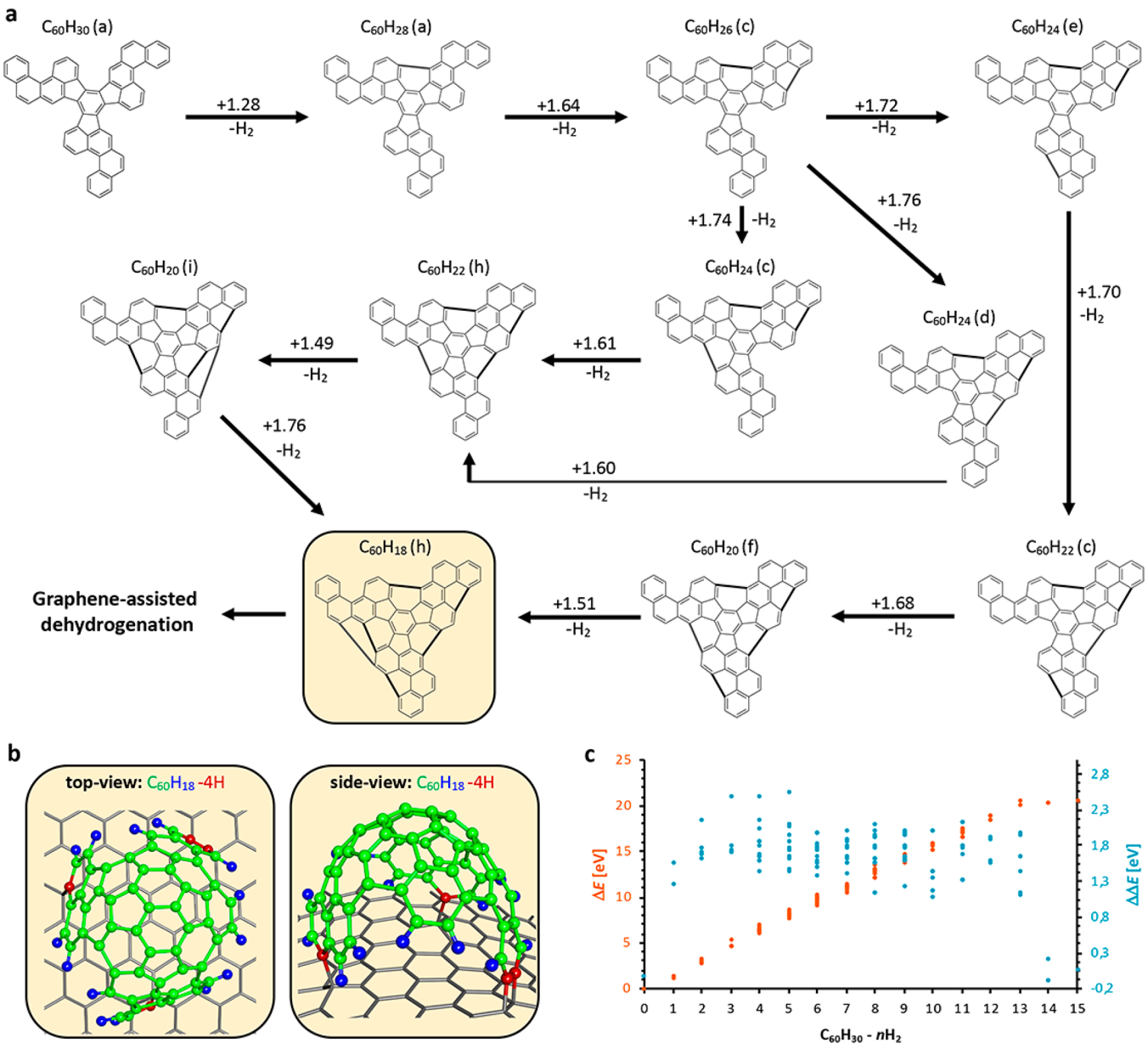

Figure 4. Thermochemical analysis of the cyclodehydrogenation reaction of 1 to C_{60}. (a) Energetically most feasible pathway to intermediate $C_{60}H_{18}$(h). Letters in brackets indicate the isomer; energy values indicated in eV. (b) Model of $C_{60}H_{18}$(h) bound to graphene; same model as in Figure 3b. Carbon skeleton indicated in green, hydrogen atoms in blue, carbon atoms bound to graphene surface in red. (c) Summary of the complete thermochemical analysis (105 considered intermediates); energies calculated at the M06-2X-def2-TZVP level of theory.

E_d, for the hydrogen and carbon atoms in **1** and C_{60} as summarized in Table S4. Hereby, two types of hydrogen atoms are found for **1**: weaker bound ($E_d \approx 7.6$ eV) H atoms in the respective *fjord* and *cove* regions,[48] and stronger bound ($E_d \approx 7.9$ eV) H atoms in the periphery. Yet, both atoms can be irreversibly displaced by the electron beam. On the other hand, the carbon atoms can be categorized into displaceable ($E_d \approx 12$ eV) secondary carbon atoms, and stable ($E_d > 17$ eV) tertiary carbon atoms. Thus, concerning possible reaction pathways, we considered the two energetically most feasible mechanisms: (1) Knock-on induced homolytic C−H bond cleavage to two $C^{\bullet}$ radicals at the subsequent dispense of one H_2 molecule, followed by radical−radical C−C bond formation. (2) Thermally allowed 6π-electrocyclization reaction, followed by aromatization through H_2 elimination. Both reaction pathways proceed *via* one intermediate structure, and we considered for both pathways the concerted elimination of one H_2 molecule. A stepwise loss of H atoms is energetically more demanding, proceeding through several intermediate steps, and is therefore not considered.

As it can be extracted from Figure 6a, the calculated energy barriers suggest that the initial cyclization step should proceed *via* an electrocyclization reaction, followed by re-aromatization,[19] rather than a 2-fold homolytic C−H bond cleavage, followed by radical recombination.[22] However, apart from the reaction barriers, it is more important to consider the cross section for each event. Therefore, we calculated the knock-on displacement cross section for each type of atom using the McKinley Feshbach approximation for isotropic knock-on threshold energies, E_d, as depicted in eq 3 in Figure 6b.[49] While the knock-on removal of atoms has no energetic upper limit, the electrocyclization pathway is limited by the threshold

https://doi.org/10.1021/acsnano.1c02222
ACS Nano 2021, 15, 12804−12814

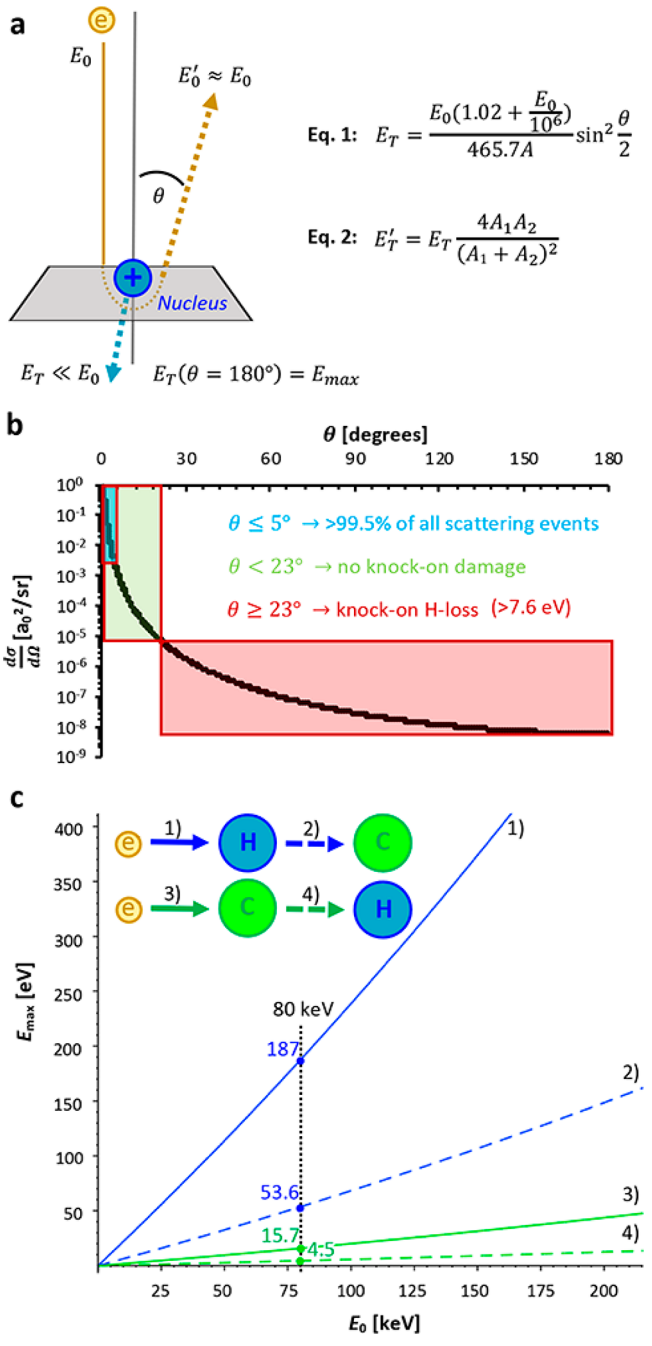

Figure 5. Elastic scattering and knock-on energy transfer relationship. (a) Schematic depiction of momentum transfer from an incoming electron to an atomic nucleus. (b) Differential elastic-scattering cross section for hydrogen at 80 kV. (c) Maximum transferred energy as a function of the electron's kinetic energy; solid lines: direct energy transfer, dashed lines: secondary energy transfer. E_T, transferable kinetic energy; E_T', secondary transferable kinetic energy; E_{max}, maximum transferable kinetic energy; E_0, kinetic energy of primary electron; A, atomic mass number; θ, elastic scattering angle.

barrier for the homolytic bond cleavage. Thus, to estimate the cross section for the cyclodehydrogenation (CDH) process σ_{CDH} *via* electrocyclization, we estimated σ_{CDH} from the difference between the cross sections of the lower (E_{TS2} = 3.1 eV, σ_{TS2}(C) = 393 barn) and upper (E_d(H) = 7.6 eV, σ_d(H) = 67 barn) threshold limits, which define the energy window for the CDH process. The respective cross sections are depicted in Figure 6c. The total electron dose for an event (TED_{ev}) to occur can be estimated by $TED_{ev} = (n\sigma)^{-1}$, in which n is the number of equivalent atoms.[50] With σ_d(H) = 67 barn for the weakest C−H bond in hand, a $TED_d = 5.0 \times 10^7$ e$^-$ nm^{-2} (C_3 symmetry, n = 3) for the first H loss *via* knock-on displacement can be estimated (for a complete list of calculated cross sections and TEDs for all atoms, refer to Table S4 in the Supporting Information). On the other hand, with σ_{CDH} (**1**) = 326 barn, the expected $TED_{CDH} = 3.1 \times 10^7$ e$^-$ nm^{-2}. This correlation stands in very good agreement with the experimental finding of intermediate $C_{60}H_{14}$ (**$C_{60}H_{18}$(h)**), which is observed at a TED = 2.8×10^7 e$^-$ nm^{-2} (compare Figure 7a).

From this point on, however, the reaction pathway does not follow the classical organic reaction pathway anymore, because the intermediate undergoes a dynamic interplay with the GML. In particular, the on-surface migration of the spherical intermediate as depicted in Figure 3c can be directly correlated to an increased hydrogen loss rate (highlighted in Figure 7a). This dynamic bond breaking and binding to the GML catalyzes the H loss significantly and makes graphene a non-innocent substrate in our observations.[51] This finding is important because previous SMART-EM studies revealed that molecules encapsulated in carbon nanotubes,[52,53] or attached to the periphery of carbon nanohorns,[15,54,55] show only minor interactions with the substrate. Even though the hydrogen atoms' contributions are neglectable to the overall contrast of the molecule in TEM, their presence (or absence) has a great impact on the overall geometry of the structure. This is subsequently reflected in the simulations in Figure 7b,c, which confirm the excessive hydrogen loss to a heavily dehydrogenated reactive intermediate (compare Figure 3e−g).

Because the observed structures of chemisorbed **1**, its key intermediates, and the final C_{60} structure match well with the simulations and models that are in line with the DFT calculations, a rearrangement of the carbon-skeleton by Stone−Wales rearrangement to an unstable non-IPR (isolated pentagon rule) isomer,[56] or knock-on removal of carbon atoms to unstable C_{60-n} (n = 1, 2, *etc.*) structures, can be ruled out.[57]

CONCLUSION

In summary, we demonstrated the video analysis of the electron-beam-induced molecule-to-molecule transformation of truxene derivative **1** ($C_{60}H_{30}$), which undergoes a preprogrammed C−C bond formation in a formal 15-fold oxidative cyclodehydrogenation reaction to fullerene C_{60}. Our detailed analysis of key intermediates and DFT calculations indicate that electron-beam-driven reactions can follow the rational design of common organic textbook chemistry. In particular, if the interaction with the substrate does not interfere, the pathway of the cyclodehydrogenation reaction appears to prefer the route *via* an electrocyclization, followed by rearomatization, rather than the homolytic C−H bond cleavage, followed by radical recombination. Hence, the product formation is primarily kinetically controlled. On the other hand, the interfering interactions of the graphene substrate with the molecular intermediates lead to a non-classical reaction pathway *via* heavily dehydrogenated intermediates. This pathway might be further accompanied by knock-on induced C−H bond cleavages, leading to the thermodynamically controlled product. From an efficiency point of view, the *in situ* fixation of organic molecules in the TEM to the graphene monolayer is rather poor, which is also

https://doi.org/10.1021/acsnano.1c02222
ACS Nano 2021, 15, 12804−12814

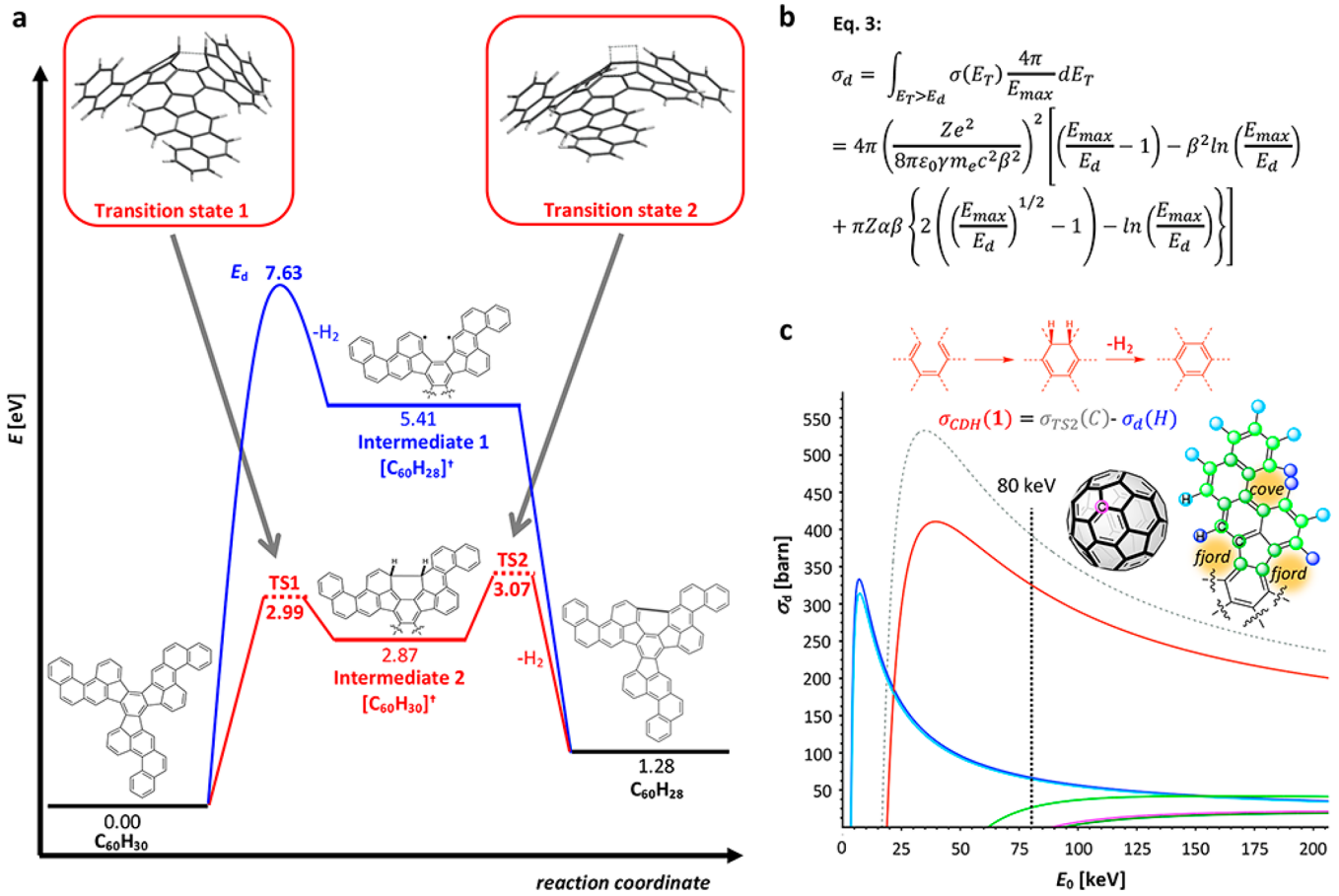

Figure 6. Computational rationalization of C−C bond formation. (a) Energy diagram for the first cyclodehydrogenation step; blue: homolytic CH-bond cleavage, followed by radical recombination; red: electrocyclization reaction, followed by aromatization *via* H_2 elimination. Energies calculated at the M06-2X-def2-TZVP level of theory. (b) McKinley Feshbach approximation for the calculation of the knock-on displacement cross section. (c) Knock-on displacement cross section as a function of the electron's kinetic energy; displayed for the weakest and strongest bound hydrogen (blue) and carbon (green) atoms in 1, as well as the carbon atom in C_{60} (magenta). E_T, transferable kinetic energy; E_d, threshold energy for knock-on removal; E_{max}, maximum transferable kinetic energy; σ_d, knock-on cross section; Z, nuclear charge; ε_0, vacuum permittivity; m_e, mass of electron; γ, Lorentz factor $\left(1/\sqrt{1-\beta^2}\right)$; c, speed of light; β, relativistic factor for the electron $\left(\sqrt{1-(1+E_0/m_e c^2)^{-2}}\right)$; α, fine structure constant.

why only a few examples in the literature are known, in which molecules were studied on the GML by *in situ* TEM before.[21,58,59] The molecules tend to bind to defect sites, glassy carbon layers, or other forms of debris, which makes it difficult to comprehend the chemistry. However, once the molecule is found as a singular, isolated entity on the surface and does not detach from it (compare Video S3), it allows us to solely focus on the molecule's dynamics without the interference of other molecules or environmental influences. The possibility to predict chemical reactions induced in the electron microscope implies that the outcome of electron-beam-initiated reactions can be rationalized from an organic chemist's point of view and controlled with careful molecular precursor design. Thus, with advancing EM technologies toward better resolution and increased sensitivities of the detectors, this will not only allow studying the fundamentals of dynamic chemical events of single molecules that relate for instance to outer space chemistry[60] but also further advance the forthcoming of the precursor design for precise nanostructures, fabricated by electron beam lithography.

METHODS

TEM Grid Preparation. CVD-grown monolayer graphene-coated quantifoil gold grids, with a hole size of 2 μm and space between the hole of 4 μm, were purchased from Graphenea. Before usage, the graphene grids were purified with activated carbon, using a modified dry-cleaning protocol.[42] The activated carbon was dried before usage at 623 K for 12 h under an ambient atmosphere. A small amount of dried activated carbon was placed into a Petri dish; the graphene grid was carefully placed atop and then fully covered with another portion of activated carbon. The Petri dish was placed in a furnace under ambient conditions and annealed in the following order: (1) heating: rt → 483 K (45 min, 4.6 K/min); (2) hold: 483 K (30 min); (3) cooling: 483 → 393 K (30 min; −3 K/min). The grid was stored at 393 K under activated carbon until it was used for the sample preparation.

Sample Preparation. For the sample preparation, the grid was mechanically cleaned from the activated carbon, using a gentle stream of dry N_2 for several minutes. Toluene and MeOH (special grade) for TEM-sample preparation were purchased from Wako Pure Chemical Industries. 10^{-5} M solutions of **1** were freshly prepared before drop-casting. Excess sample solution was removed with a filter paper. The sample grid was further cleaned with two cycles of one drop of MeOH, followed by removal with a filter paper. The grid was then

https://doi.org/10.1021/acsnano.1c02222
ACS Nano 2021, 15, 12804−12814

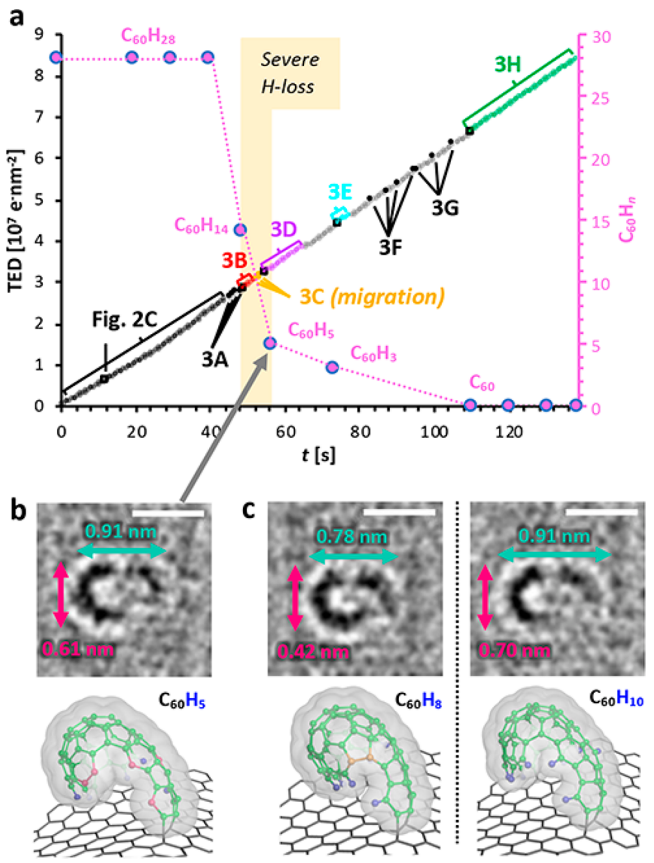

Figure 7. Analysis of the cyclodehydrogenation process. (a) Event analysis as a function of time; plot of TED against time. Colored data points indicate the TEM images from Figures 2 and 3; secondary axis (magenta) shows the hydrogen loss over time, as determined from the simulated models. (b) Best-fitting simulation and model for $C_{60}H_5$ for the TEM image in Figure 3d. (c) Alternative models with different hydrogen atom content and respective simulations.

predried in high vacuum at 5×10^{-5} Pa for 1 h, before introducing the sample into the TEM chamber.

TEM Observation and Image Analysis. Atomic-resolution EM observations were carried out on a JEOL JEM-ARM200F instrument, equipped with an aberration corrector, at an acceleration voltage of 80 kV and a vacuum of 1×10^{-5} Pa in the specimen chamber. The microscope is placed on an antivibration base plate which, in turn, is placed on a 5 m thick concrete bedding to minimize mechanical vibrations. Experiments were carried out on a heating holder (JEOL EM-21130). The accuracy of the grid temperature is ± a few degrees according to the instrumental specification. To remove volatile impurities from the specimen, the holder was heated at 473 K for 60 min without electron irradiation before cooling to 298 ± 5 K. After the stage temperature settled to the target value, we waited for an additional 30 min to minimize thermal drift. EM videos were recorded on a CMOS camera (Gatan OneView, 4096 × 4096 pixels) operated in binning 2 mode (output image size: 2048 × 2048 pixels, pixel resolution 0.021 nm at ×1 000 000), with an exposure time of 250 ms and a frame rate of 2 fps. All images were automatically processed on Gatan DigitalMicrograph software. The images were collected in the .dm3 format on Gatan DigitalMicrograph software and processed using ImageJ 1.51f software.[61] To remove the unevenness of the electron irradiation, all images were processed by a band-pass filter (filtering structures smaller than 3 pixels and larger than 40 pixels, tolerance of direction: 5%), Gaussian blurred (sigma radius 1.0), and contrast/brightness adjusted. Before analysis, images were subjected to a thermal drift correction.

TEM Simulations. TEM simulation images were electron dose corrected, according to the electron dose rate from the TEM experiment, and generated by using a multi-slice procedure implemented in the Bionet elbis software.[62] Simulation parameters were set to agree with the actual experimental parameters: acc. Volt. = 80.00 kV, λ = 0.04176 Å, Cs = −0.003 mm, df = 160 Å, Cc = 1.25 mm, de = 0.60 eV, α = 0.20 mrad, OL Aperture radius = 20.88 mrad, OL Aperture radius = 0.50 Å^{-1}, pixel size = 0.0210844, max. Intens. = 1.1278. The simulation images were processed analogously to the experimental TEM images, to obtain the best correlation.

Computational Analysis. Geometry optimization and energy calculations were carried out using the SPARTAN '18 work package.[63,64] Structures were optimized on the semi-empirical level PM6 and then further refined at the density functional theory level, using the Minnesota global hybrid meta generalized gradient approximation functional M06-2X with 54% Hartree−Fock exchange.[65] For comparison reasons, reactions regarding the thermochemical pathway of $C_{60}H_{30}$ and the bond dissociation energy of coronene, calculations were further carried out using B3LYP[66,67] and ωB97X-D[68] as functionals. Geometry optimization and initial evaluation of the molecules' energies were performed with the Pople-type dual basis split-valence triple-ζ/double-ζ quality basis set 6-311G(d,p)[6-31G(d)]. Final energy calculations for the thermochemical evaluation were carried out using the M06-2X functional with the Ahlrichs-Weigend triple-ζ quality basis set def2-TZVP.[69] Transition state geometries were obtained at the M06-2X/6-31G(d) DFT level of theory and confirmed by identification of the imaginary frequency. Respective energies were obtained at the M06-2X/def2-TZVP level of theory. Bond threshold energies were calculated at the M06-2X/def2-TZVP level of theory and compared to values obtained from ωB97X-D/6-311G(d) for coronene.[22]

ASSOCIATED CONTENT

Supporting Information

The Supporting Information is available free of charge at https://pubs.acs.org/doi/10.1021/acsnano.1c02222.

Detailed experimental and theoretical procedures and additional discussions (PDF)

Video S1: Transformation of **1** to C_{60} on graphene (AVI)

Video S2: The fullerene bound to the graphene layer (AVI)

Video S3: Detachment of **1** from graphene layer (AVI)

AUTHOR INFORMATION

Corresponding Authors

Dominik Lungerich − *Center for Nanomedicine (CNM), Institute for Basic Science (IBS), Seoul 03722, South Korea; Graduate Program of Nano Biomedical Engineering (NanoBME), Advanced Science Institute, Yonsei University, Seoul 03722, South Korea; Department of Chemistry, The University of Tokyo, Tokyo 113-0033, Japan;* orcid.org/0000-0002-3093-3624; Email: d.lungerich@yonsei.ac.kr

Eiichi Nakamura − *Department of Chemistry, The University of Tokyo, Tokyo 113-0033, Japan;* orcid.org/0000-0002-4192-1741; Email: nakamura@chem.s.u-tokyo.ac.jp

Authors

Helen Hoelzel − *Department of Chemistry, The University of Tokyo, Tokyo 113-0033, Japan; Department of Chemistry and Pharmacy, Organic Chemistry II, Friedrich-Alexander-University Erlangen-Nuernberg (FAU), 91058 Erlangen, Germany;* Present Address: Department of Chemistry and Chemical Engineering, Chalmers University of Technology, 41296 Gothenburg, Sweden.; orcid.org/0000-0003-2312-9934

https://doi.org/10.1021/acsnano.1c02222
ACS Nano 2021, 15, 12804−12814

Koji Harano − *Department of Chemistry, The University of Tokyo, Tokyo 113-0033, Japan;* orcid.org/0000-0001-6800-8023

Norbert Jux − *Department of Chemistry and Pharmacy, Organic Chemistry II, Friedrich-Alexander-University Erlangen-Nuernberg (FAU), 91058 Erlangen, Germany;* orcid.org/0000-0002-5673-8181

Konstantin Yu. Amsharov − *Department of Chemistry, Martin-Luther-University Halle-Wittenberg, 06120 Halle, Germany;* orcid.org/0000-0002-2854-8081

Complete contact information is available at: https://pubs.acs.org/10.1021/acsnano.1c02222

Author Contributions

D.L. wrote the manuscript with feedback from all authors. All the authors discussed the results and commented on the manuscript. D.L. conceptualized and developed the project. D.L., N.J., and E.N. supervised the project. H.H. and D.L. developed the method. D.L. carried out the TEM experiments and data analysis, provided the software, and carried out DFT calculations and EM simulations. K.Y.A. synthesized and provided precursor **1**. K.H. and E.N. were responsible for data storage and providing access and maintenance of the TEM. E.N., N.J., and D.L. were responsible for funding acquisition. All authors approved the final version of the manuscript.

Notes

The authors declare no competing financial interest.

ACKNOWLEDGMENTS

The research was supported by the Institute for Basic Science (IBS-R026-Y1), JSPS (KAKENHI JP19H05459), Japan Science and Technology Agency (CREST JPMJCR20B2), and the Deutsche Forschungsgemeinschaft (DFG, Projektnummer 182849149, SFB 953). H.H. and D.L. acknowledge the support as an International Research Fellow from the Japan Society for the Promotion of Science (JSPS). H.H. further thanks the Bavarian Equal Opportunities Sponsorship − Realisierung von Chancengleichheit von Frauen in Forschung und Lehre (FFL) − Realization Equal Opportunities for Women in Research and Teaching, for financial support. D.L. further thanks the Alexander von Humboldt Foundation (AvH) for a Feodor-Lynen return fellowship, and IBS for funding. Mr. J. Y. Yoon (IBS) is thanked for helpful discussions.

REFERENCES

(1) Kroto, H. W.; Heath, J. R.; O'Brien, S. C.; Curl, R. F.; Smalley, R. E. C_{60}: Buckminsterfullerene. *Nature* **1985**, *318*, 162−163.

(2) Zieleniewska, A.; Lodermeyer, F.; Roth, A.; Guldi, D. M. Fullerenes-How 25 Years of Charge Transfer Chemistry Have Shaped Our Understanding of (Interfacial) Interactions. *Chem. Soc. Rev.* **2018**, *47*, 702−714.

(3) Lebedeva, M. A.; Chamberlain, T. W.; Khlobystov, A. N. Harnessing the Synergistic and Complementary Properties of Fullerene and Transition-Metal Compounds for Nanomaterial Applications. *Chem. Rev.* **2015**, *115*, 11301−11351.

(4) Hong, G.; Diao, S.; Antaris, A. L.; Dai, H. Carbon Nanomaterials for Biological Imaging and Nanomedicinal Therapy. *Chem. Rev.* **2015**, *115*, 10816−10906.

(5) Rubin, Y. Organic Approaches to Endohedral Metallofullerenes: Cracking Open or Zipping up Carbon Shells? *Chem. - Eur. J.* **1997**, *3*, 1009−1016.

(6) Scott, L. T.; Boorum, M. M.; McMahon, B. J.; Hagen, S.; Mack, J.; Blank, J.; Wegner, H.; de Meijere, A. A Rational Chemical Synthesis of C_{60}. *Science* **2002**, *295*, 1500−1503.

(7) Boorum, M. M.; Vasil'ev, Y. V.; Drewello, T.; Scott, L. T. Groundwork for a Rational Synthesis of C_{60}: Cyclodehydrogenation of a $C_{60}H_{30}$ Polyarene. *Science* **2001**, *294*, 828−831.

(8) Otero, G.; Biddau, G.; Sánchez-Sánchez, C.; Caillard, R.; López, M. F.; Rogero, C.; Palomares, F. J.; Cabello, N.; Basanta, M. A.; Ortega, J.; Méndez, J.; Echavarren, A. M.; Pérez, R.; Gómez-Lor, B.; Martín-Gago, J. A. Fullerenes from Aromatic Precursors by Surface-Catalysed Cyclodehydrogenation. *Nature* **2008**, *454*, 865−868.

(9) Gross, L.; Schuler, B.; Pavliček, N.; Fatayer, S.; Majzik, Z.; Moll, N.; Peña, D.; Meyer, G. Atomic Force Microscopy for Molecular Structure Elucidation. *Angew. Chem., Int. Ed.* **2018**, *57*, 3888−3908.

(10) Ruffieux, P.; Wang, S.; Yang, B.; Sanchez-Sanchez, C.; Liu, J.; Dienel, T.; Talirz, L.; Shinde, P.; Pignedoli, C. A.; Passerone, D.; Dumslaff, T.; Feng, X.; Mullen, K.; Fasel, R. On-Surface Synthesis of Graphene Nanoribbons with Zigzag Edge Topology. *Nature* **2016**, *531*, 489−492.

(11) Sanchez-Valencia, J. R.; Dienel, T.; Gröning, O.; Shorubalko, I.; Mueller, A.; Jansen, M.; Amsharov, K. Y.; Ruffieux, P.; Fasel, R. Controlled Synthesis of Single-Chirality Carbon Nanotubes. *Nature* **2014**, *512*, 61−64.

(12) Gröning, O.; Wang, S.; Yao, X.; Pignedoli, C. A.; Borin Barin, G.; Daniels, C.; Cupo, A.; Meunier, V.; Feng, X.; Narita, A.; Müllen, K.; Ruffieux, P.; Fasel, R. Engineering of Robust Topological Quantum Phases in Graphene Nanoribbons. *Nature* **2018**, *560*, 209−213.

(13) Nakamura, E. Atomic-Resolution Transmission Electron Microscopic Movies for Study of Organic Molecules, Assemblies, and Reactions: The First 10 Years of Development. *Acc. Chem. Res.* **2017**, *50*, 1281−1292.

(14) Skowron, S. T.; Chamberlain, T. W.; Biskupek, J.; Kaiser, U.; Besley, E.; Khlobystov, A. N. Chemical Reactions of Molecules Promoted and Simultaneously Imaged by the Electron Beam in Transmission Electron Microscopy. *Acc. Chem. Res.* **2017**, *50*, 1797−1807.

(15) Xing, J.; Schweighauser, L.; Okada, S.; Harano, K.; Nakamura, E. Atomistic Structures and Dynamics of Prenucleation Clusters in MOF-2 and MOF-5 Syntheses. *Nat. Commun.* **2019**, *10*, 3608.

(16) Shimizu, T.; Lungerich, D.; Stuckner, J.; Murayama, M.; Harano, K.; Nakamura, E. Real-Time Video Imaging of Mechanical Motions of a Single Molecular Shuttle with Sub-Millisecond Sub-Angstrom Precision. *Bull. Chem. Soc. Jpn.* **2020**, *93*, 1079−1085.

(17) Chuvilin, A.; Kaiser, U.; Bichoutskaia, E.; Besley, N. A.; Khlobystov, A. N. Direct Transformation of Graphene to Fullerene. *Nat. Chem.* **2010**, *2*, 450−453.

(18) Koshino, M.; Niimi, Y.; Nakamura, E.; Kataura, H.; Okazaki, T.; Suenaga, K.; Iijima, S. Analysis of the Reactivity and Selectivity of Fullerene Dimerization Reactions at the Atomic Level. *Nat. Chem.* **2010**, *2*, 117−124.

(19) Okada, S.; Kowashi, S.; Schweighauser, L.; Yamanouchi, K.; Harano, K.; Nakamura, E. Direct Microscopic Analysis of Individual C_{60} Dimerization Events: Kinetics and Mechanisms. *J. Am. Chem. Soc.* **2017**, *139*, 18281−18287.

(20) Biskupek, J.; Skowron, S. T.; Stoppiello, C. T.; Rance, G. A.; Alom, S.; Fung, K. L. Y.; Whitby, R. J.; Levitt, M. H.; Ramasse, Q. M.; Kaiser, U.; Besley, E.; Khlobystov, A. N. Bond Dissociation and Reactivity of HF and H_2O in a Nano Test Tube. *ACS Nano* **2020**, *14*, 11178−11189.

(21) Chamberlain, T. W.; Biskupek, J.; Skowron, S. T.; Markevich, A. V.; Kurasch, S.; Reimer, O.; Walker, K. E.; Rance, G. A.; Feng, X.; Müllen, K.; Turchanin, A.; Lebedeva, M. A.; Majouga, A. G.; Nenajdenko, V. G.; Kaiser, U.; Besley, E.; Khlobystov, A. N. Stop-Frame Filming and Discovery of Reactions at the Single-Molecule Level by Transmission Electron Microscopy. *ACS Nano* **2017**, *11*, 2509−2520.

(22) Chamberlain, T. W.; Biskupek, J.; Skowron, S. T.; Bayliss, P. A.; Bichoutskaia, E.; Kaiser, U.; Khlobystov, A. N. Isotope Substitution

Extends the Lifetime of Organic Molecules in Transmission Electron Microscopy. *Small* **2015**, *11*, 622−629.
(23) Carini, M.; Shi, L.; Chamberlain, T. W.; Liu, M.; Valenti, G.; Melle Franco, M.; Paolucci, F.; Khlobystov, A. N.; Pichler, T.; Mateo Alonso, A. Wall- and Hybridisation-Selective Synthesis of Nitrogen-Doped Double-Walled Carbon Nanotubes. *Angew. Chem., Int. Ed.* **2019**, *58*, 10276−10280.
(24) Botos, A.; Biskupek, J.; Chamberlain, T. W.; Rance, G. A.; Stoppiello, C. T.; Sloan, J.; Liu, Z.; Suenaga, K.; Kaiser, U.; Khlobystov, A. N. Carbon Nanotubes as Electrically Active Nanoreactors for Multi-Step Inorganic Synthesis: Sequential Transformations of Molecules to Nanoclusters and Nanoclusters to Nanoribbons. *J. Am. Chem. Soc.* **2016**, *138*, 8175−8183.
(25) Cao, K.; Chamberlain, T. W.; Biskupek, J.; Zoberbier, T.; Kaiser, U.; Khlobystov, A. N. Direct Correlation of Carbon Nanotube Nucleation and Growth with the Atomic Structure of Rhenium Nanocatalysts Stimulated and Imaged by the Electron Beam. *Nano Lett.* **2018**, *18*, 6334−6339.
(26) Cao, K.; Biskupek, J.; Stoppiello, C. T.; McSweeney, R. L.; Chamberlain, T. W.; Liu, Z.; Suenaga, K.; Skowron, S. T.; Besley, E.; Khlobystov, A. N.; Kaiser, U. Atomic Mechanism of Metal Crystal Nucleus Formation in a Single-Walled Carbon Nanotube. *Nat. Chem.* **2020**, *12*, 921−928.
(27) Cao, K.; Skowron, S. T.; Biskupek, J.; Stoppiello, C. T.; Leist, C.; Besley, E.; Khlobystov, A. N.; Kaiser, U. Imaging an Unsupported Metal−Metal Bond in Dirhenium Molecules at the Atomic Scale. *Sci. Adv.* **2020**, *6*, No. eaay5849.
(28) Nakamuro, T.; Sakakibara, M.; Nada, H.; Harano, K.; Nakamura, E. Capturing the Moment of Emergence of Crystal Nucleus from Disorder. *J. Am. Chem. Soc.* **2021**, *143*, 1763−1767.
(29) Allen, C. S.; Ito, Y.; Robertson, A. W.; Shinohara, H.; Warner, J. H. Two-Dimensional Coalescence Dynamics of Encapsulated Metallofullerenes in Carbon Nanotubes. *ACS Nano* **2011**, *5*, 10084−10089.
(30) Nakamura, E.; Koshino, M.; Saito, T.; Niimi, Y.; Suenaga, K.; Matsuo, Y. Electron Microscopic Imaging of a Single Group 8 Metal Atom Catalyzing C−C Bond Reorganization of Fullerenes. *J. Am. Chem. Soc.* **2011**, *133*, 14151−14153.
(31) Ran, K.; Zuo, J.-M.; Chen, Q.; Shi, Z. Electron Beam Stimulated Molecular Motions. *ACS Nano* **2011**, *5*, 3367−3372.
(32) Warner, J. H.; Plant, S. R.; Young, N. P.; Porfyrakis, K.; Kirkland, A. I.; Briggs, G. A. D. Atomic Scale Growth Dynamics of Nanocrystals within Carbon Nanotubes. *ACS Nano* **2011**, *5*, 1410−1417.
(33) Chuvilin, A.; Khlobystov, A. N.; Obergfell, D.; Haluska, M.; Yang, S.; Roth, S.; Kaiser, U. Observations of Chemical Reactions at the Atomic Scale: Dynamics of Metal-Mediated Fullerene Coalescence and Nanotube Rupture. *Angew. Chem., Int. Ed.* **2010**, *49*, 193−196.
(34) Warner, J. H.; Wilson, M. Elastic Distortions of Carbon Nanotubes Induced by Chiral Fullerene Chains. *ACS Nano* **2010**, *4*, 4011−4016.
(35) Koyama, T.; Fujiki, K.; Nagasawa, Y.; Okada, S.; Asaka, K.; Saito, Y.; Kishida, H. Different Molecular Arrangement of Perylene in Metallic and Semiconducting Carbon Nanotubes: Impact of van der Waals Interaction. *J. Phys. Chem. C* **2018**, *122*, 5805−5812.
(36) Botka, B.; Füstös, M. E.; Tóháti, H. M.; Németh, K.; Klupp, G.; Szekrényes, Z.; Kocsis, D.; Utczás, M.; Székely, E.; Váczi, T.; Tarczay, G.; Hackl, R.; Chamberlain, T. W.; Khlobystov, A. N.; Kamarás, K. Interactions and Chemical Transformations of Coronene inside and outside Carbon Nanotubes. *Small* **2014**, *10*, 1369−1378.
(37) Chamberlain, T. W.; Biskupek, J.; Rance, G. A.; Chuvilin, A.; Alexander, T. J.; Bichoutskaia, E.; Kaiser, U.; Khlobystov, A. N. Size, Structure, and Helical Twist of Graphene Nanoribbons Controlled by Confinement in Carbon Nanotubes. *ACS Nano* **2012**, *6*, 3943−3953.
(38) Winter, A.; George, A.; Neumann, C.; Tang, Z.; Mohn, M. J.; Biskupek, J.; Masurkar, N.; Reddy, A. L. M.; Weimann, T.; Hübner, U.; Kaiser, U.; Turchanin, A. Lateral Heterostructures of Two-Dimensional Materials by Electron-Beam Induced Stitching. *Carbon* **2018**, *128*, 106−116.
(39) Mirzayev, R.; Mustonen, K.; Monazam, M. R. A.; Mittelberger, A.; Pennycook, T. J.; Mangler, C.; Susi, T.; Kotakoski, J.; Meyer, J. C. Buckyball Sandwiches. *Sci. Adv.* **2017**, *3*, No. e1700176.
(40) Kabdulov, M.; Jansen, M.; Amsharov, K. Y. Bottom-Up C_{60} Fullerene Construction from a Fluorinated $C_{60}H_{21}F_9$ Precursor by Laser-Induced Tandem Cyclization. *Chem. - Eur. J.* **2013**, *19*, 17262−17266.
(41) Greisch, J.-F.; Amsharov, K. Y.; Weippert, J.; Weis, P.; Böttcher, A.; Kappes, M. M. From Planar to Cage in 15 Easy Steps: Resolving the $C_{60}H_{21}F_9^- \rightarrow C_{60}^-$ Transformation by Ion Mobility Mass Spectrometry. *J. Am. Chem. Soc.* **2016**, *138*, 11254−11263.
(42) Algara-Siller, G.; Lehtinen, O.; Turchanin, A.; Kaiser, U. Dry-Cleaning of Graphene. *Appl. Phys. Lett.* **2014**, *104*, 153115.
(43) Markevich, A.; Kurasch, S.; Lehtinen, O.; Reimer, O.; Feng, X.; Müllen, K.; Turchanin, A.; Khlobystov, A. N.; Kaiser, U.; Besley, E. Electron Beam Controlled Covalent Attachment of Small Organic Molecules to Graphene. *Nanoscale* **2016**, *8*, 2711−2719.
(44) Denis, P. A.; Iribarne, F. [2 + 2] Cycloadditions onto Graphene. *J. Mater. Chem.* **2012**, *22*, 5470−5477.
(45) He, K.; Lee, G.-D.; Robertson, A. W.; Yoon, E.; Warner, J. H. Hydrogen-Free Graphene Edges. *Nat. Commun.* **2014**, *5*, 3040.
(46) Lee, J. K.; Lee, G.-D.; Lee, S.; Yoon, E.; Anderson, H. L.; Briggs, G. A. D.; Warner, J. H. Atomic Scale Imaging of Reversible Ring Cyclization in Graphene Nanoconstrictions. *ACS Nano* **2019**, *13*, 2379−2388.
(47) Tsuda, M.; Ishida, T.; Nogami, T.; Kurono, S.; Ohashi, M. Isolation and Characterization of Diels-Alder Adducts of C_{60} with Anthracene and Cyclopentadiene. *J. Chem. Soc., Chem. Commun.* **1993**, 1296−1298.
(48) Lungerich, D.; Papaianina, O.; Feofanov, M.; Liu, J.; Devarajulu, M.; Troyanov, S. I.; Maier, S.; Amsharov, K. Y. Dehydrative π-Extension to Nanographenes with Zig-Zag Edges. *Nat. Commun.* **2018**, *9*, 4756.
(49) Susi, T.; Meyer, J. C.; Kotakoski, J. Quantifying Transmission Electron Microscopy Irradiation Effects Using Two-Dimensional Materials. *Nat. Rev. Phys.* **2019**, *1*, 397−405.
(50) Santana, A.; Zobelli, A.; Kotakoski, J.; Chuvilin, A.; Bichoutskaia, E. Inclusion of Radiation Damage Dynamics in High-Resolution Transmission Electron Microscopy Image Simulations: The Example of Graphene. *Phys. Rev. B: Condens. Matter Mater. Phys.* **2013**, *87*, 094110.
(51) Navarro, J. J.; Pisarra, M.; Nieto-Ortega, B.; Villalva, J.; Ayani, C. G.; Díaz, C.; Calleja, F.; Miranda, R.; Martín, F.; Pérez, E. M.; Vázquez de Parga, A. L. Graphene Catalyzes the Reversible Formation of a C-C Bond between Two Molecules. *Sci. Adv.* **2018**, *4*, No. eaau9366.
(52) Khlobystov, A. N. Carbon Nanotubes: From Nano Test Tube to Nano-Reactor. *ACS Nano* **2011**, *5*, 9306−9312.
(53) Britz, D. A.; Khlobystov, A. N. Noncovalent Interactions of Molecules with Single Walled Carbon Nanotubes. *Chem. Soc. Rev.* **2006**, *35*, 637.
(54) Kamei, K.; Shimizu, T.; Harano, K.; Nakamura, E. Aryl Radical Addition to Curvatures of Carbon Nanohorns for Single-Molecule-Level Molecular Imaging. *Bull. Chem. Soc. Jpn.* **2020**, *93*, 1603−1608.
(55) Gorgoll, R. M.; Yücelen, E.; Kumamoto, A.; Shibata, N.; Harano, K.; Nakamura, E. Electron Microscopic Observation of Selective Excitation of Conformational Change of a Single Organic Molecule. *J. Am. Chem. Soc.* **2015**, *137*, 3474−3477.
(56) Xu, Z.; Liang, Z.; Ding, F. Isomerization of sp^2-Hybridized Carbon Nanomaterials: Structural Transformation and Topological Defects of Fullerene, Carbon Nanotube, and Graphene. *Wiley Interdiscip. Rev.: Comput. Mol. Sci.* **2017**, *7*, No. e1283.
(57) Egerton, R. F. Radiation Damage to Organic and Inorganic Specimens in the TEM. *Micron* **2019**, *119*, 72−87.
(58) Gerkman, M. A.; Sinha, S.; Warner, J. H.; Han, G. G. D. Direct Imaging of Photoswitching Molecular Conformations Using Individual Metal Atom Markers. *ACS Nano* **2019**, *13*, 87−96.
(59) Kengmana, E. S.; Lee, J. K.; Li, X.; Warner, J. H.; Han, G. G. D. Self-Assembly of Bowlic Supramolecules on Graphene Imaged at the

https://doi.org/10.1021/acsnano.1c02222
ACS Nano 2021, 15, 12804−12814

Individual Molecular Level Using Heavy Atom Tagging. *Small* **2020**, *16*, 2002860.
(60) Berné, O.; Tielens, A. G. G. M. Formation of Buckminsterfullerene (C_{60}) in Interstellar Space. *Proc. Natl. Acad. Sci. U. S. A.* **2012**, *109*, 401−406.
(61) Schneider, C. A.; Rasband, W. S.; Eliceiri, K. W. NIH Image to ImageJ: 25 Years of Image Analysis. *Nat. Methods* **2012**, *9*, 671−675.
(62) Hosokawa, F.; Shinkawa, T.; Arai, Y.; Sannomiya, T. Benchmark Test of Accelerated Multi-Slice Simulation by GPGPU. *Ultramicroscopy* **2015**, *158*, 56−64.
(63) Shao, Y.; Molnar, L. F.; Jung, Y.; Kussmann, J.; Ochsenfeld, C.; Brown, S. T.; Gilbert, A. T. B.; Slipchenko, L. V.; Levchenko, S. V.; O'Neill, D. P.; DiStasio, R. A., Jr; Lochan, R. C.; Wang, T.; Beran, G. J. O.; Besley, N. A.; Herbert, J. M.; Lin, C. Y.; Van Voorhis, T.; Chien, S. H.; Sodt, A.; et al. Advances in Methods and Algorithms in a Modern Quantum Chemistry Program Package. *Phys. Chem. Chem. Phys.* **2006**, *8*, 3172−3191.
(64) Shao, Y.; Gan, Z.; Epifanovsky, E.; Gilbert, A. T. B.; Wormit, M.; Kussmann, J.; Lange, A. W.; Behn, A.; Deng, J.; Feng, X.; Ghosh, D.; Goldey, M.; Horn, P. R.; Jacobson, L. D.; Kaliman, I.; Khaliullin, R. Z.; Kuś, T.; Landau, A.; Liu, J.; Proynov, E. I.; et al. Advances in Molecular Quantum Chemistry Contained in the Q-Chem 4 Program Package. *Mol. Phys.* **2015**, *113*, 184−215.
(65) Zhao, Y.; Truhlar, D. G. The M06 Suite of Density Functionals for Main Group Thermochemistry, Thermochemical Kinetics, Noncovalent Interactions, Excited States, and Transition Elements: Two New Functionals and Systematic Testing of Four M06-Class Functionals and 12 Other Functionals. *Theor. Chem. Acc.* **2008**, *120*, 215−241.
(66) Stephens, P. J.; Devlin, F. J.; Chabalowski, C. F.; Frisch, M. J. *Ab Initio* Calculation of Vibrational Absorption and Circular Dichroism Spectra Using Density Functional Force Fields. *J. Phys. Chem.* **1994**, *98*, 11623−11627.
(67) Becke, A. D. Density-Functional Thermochemistry. III. The Role of Exact Exchange. *J. Chem. Phys.* **1993**, *98*, 5648−5652.
(68) Chai, J.-D.; Head-Gordon, M. Long-Range Corrected Hybrid Density Functionals with Damped Atom-Atom Dispersion Corrections. *Phys. Chem. Chem. Phys.* **2008**, *10*, 6615−6620.
(69) Weigend, F.; Ahlrichs, R. Balanced Basis Sets of Split Valence, Triple Zeta Valence and Quadruple Zeta Valence Quality for H to Rn: Design and Assessment of Accuracy. *Phys. Chem. Chem. Phys.* **2005**, *7*, 3297−3305.

https://doi.org/10.1021/acsnano.1c02222
ACS Nano 2021, 15, 12804−12814